Wind and Structures, *Vol. 29, No. 2 (2019) 99-110*
DOI: https://doi.org/10.12989/was.2019.29.2.099

An integrated optimal design of energy dissipation structures under wind loads considering SSI effect

Xuefei Zhao*[1], Han Jiang[1a] and Shuguang Wang[2b]

[1]*Nanjing Yangtze River Urban Architectural Design Co., LTD., Nanjing 210000, China*
[2]*College of Civil engineering, Nanjing Tech University ,Nanjing 210000, China*

(Received March 7, 2018, Revised December 20, 2018, Accepted December 28, 2019)

Abstract. This paper provides a simple numerical method to determine the optimal parameters of tuned mass damper (TMD) and viscoelastic dampers (VEDs) in frame structure for wind vibration control considering the soil-structure interation (SSI) effect in frequency domain. Firstly, the numerical model of frame structure equipped with TMD and VEDs considering SSI effect is established in frequency domain. Then, the genetic algorithm (GA) is applied to obtain the optimal parameters of VEDs and TMD. The optimization process is demonstrated by a 20-storey frame structure supported by pile group for different soil conditions. Two wind resistant systems are considered in the analysis, the Structure-TMD system and the Structure-TMD-VEDs system. The example proves that this method can quickly determine the optimal parameters of energy dissipation devices compared with the traditional finite element method, thus is practically valuable.

Keywords: viscoelastic damper; tuned mass damper; soil structure interaction; genetic algorithm; optimization

1. Introduction

In recent years, more and more light weight and high strength materials are applied to tall buildings. These structures are generally more flexible and have low damping, which may bring about excessive wind-induced vibration. For such a case, many control theories and auxiliary devices have been proposed or applied to control the wind induced vibration of tall buildings.

One of the commonly used control devices is a tuned mass damper (TMD). The TMD is a vibration absorbing equipment consisting of mass, springs and damping devices. Its frequency can be tuned to match the predominant vibration frequency (usually the fundamental natural frequency) of the main structure. Accordingly, the structural dynamic responses caused by environmental excitation, such as strong winds or earthquakes, can be significantly reduced.

Currently, many studies have been devoted to finding the optimum parameters of TMD and evaluating its efficiency under various types of dynamic excitation. Den Hartog (1947) and Brock (1946) have given the optimum TMD parameters excited by harmonic external forces in order to minimize the displacement of a single degree-of-freedom (SDOF) main structure. Warburton and Ayorinde (1980) have proved the accuracy of simplifying the multi degree-of-freedom (MDOF) system with TMD as a SDOF system through a large number of numerical examples, such as plates, beams and shells.

Chang (1999) have proposed the approximate form of optimum TMD tuning expressions for wind and earthquakeexcitation. Lots of numerical optimization algorithms have also been used for obtaining the optimal parameters of TMD. Genetic algorithm (GA) is the most employed algorithm (Arfiadi *et al*. 1998, Singh *et al.* 2002., Desu *et al.* 2006, Pourzeynali *et al*. 2008, Marano *et al.* 2010). Besides, the particle swarm optimization (Leung *et al.* 2008, 2009), bionic algorithm (Steinbuch 2011), and harmony search algorithm are also applied for TMD optimization (Bekdaş and Nigdeli 2011).

In addition to TMD, various types of energy dissipation devices, such as viscoelastic damper (VED), viscous fluid damper and friction damper, have also been used for vibration control of structures in recent years (Zhang and Soong 1992, Chang and Lin 2004, Hwang *et al.* 2008, Lewandowski *et al.* 2012). Among these devices, the VED is the most commonly used damper in structure for wind induced vibration control due to the cost-effectiveness and high reliability.

For the complexity of the dynamic soil structure interaction (SSI) analysis, most optimal designs of TMD or VED are based on the rigid foundation assumption. However, the dynamic responses of high-rise buildings founded on relatively soft soil may be different from those based on rigid foundations. The studies of Veletsos (1974), Avilés (1999) and Medina (2013) have demonstrated that the SSI effect significantly modify the structural dynamic characteristics, especially the natural frequency, which has a great effect on the responses of structures excited by earthquakes or winds. On the one hand, the dynamic properties of VED and TMD are closely related to the natural frequency of the structural system, which will be inevitably influenced by the SSI effect. On the other hand,

*Corresponding author, Ph.D.
E-mail: zhaoxuefeinjut@163.com
[a] Ph.D.
[b] Ph.D.

ISSN: 1226-6116 (Print), 1598-6225 (Online)

the stiffness and damping changes of the structural system caused by the added vibration control devices will affect the SSI effect in turn. Accordingly, the dynamic analysis of the structure with VEDs or TMD considering SSI effect is a complicated coupling problem. The assumption of rigid foundation may result in analytical inaccuracy and considerable deviation from the original design objective if the structures equipped with VEDs or TMD are built on relatively soft foundations.

At present, there are many studies concerning the parameter optimal design of TMD or VED used in structures for wind induced vibration control based on rigid foundation assumptions. However, an integrated optimal use of VEDs and TMD in structure considering the SSI effect is rarely seen. In this paper, the mathematical model of a wind resistant frame structural system equipped with both TMD and VEDs within consideration of SSI effect is firstly established in frequency domain. Then, the GA is used as a numerical searching technique to find the the optimal parameters of TMD and VEDs. A pile group supported 20-storey frame structure is used as a numerical example to demonstrate the optimization procedure for different soil conditions. The studies of this paper will provide a rapid determination of the optimal parameters of TMD and VEDs for wind vibration control of frame structures considering the SSI effect.

2. The constitutive model of VED

The five-parameter Fractional derivative Maxwell (FDM) model is used in this paper to demonstrate the general behavior of the viscoelastic damper. The model was first proposed by Makris and Constantinous (1991) and very good agreement between the predicted and experimental results were obtained over a wide range of frequency. The general force-displacement constitutive equation of the model can be expressed as

$$P(t)+b_0D^{\beta}[P(t)]=k_0u(t)+c_0D^{\alpha}[u(t)] \tag{1}$$

where t is the time, $P(t)$ is the damping force, and $u(t)$ is the damper deformation. b_0,α,β,k_0,c_0 are material constants with constraint $0\le\beta,\alpha\le 1$ .The fractional derivative order $D^{\alpha}[],D^{\beta}[]$ can be defined by an integral form expressed as follows

$$D^{\alpha}[f(t)]=\frac{d^{\alpha}f(t)}{dt^{\alpha}}=\frac{1}{\Gamma(1-\alpha)}\frac{d}{dt}\left[\int_0^t\frac{f(\tau)}{(t-\tau)^{\alpha}}d\tau\right] \tag{2}$$

$$D^{\beta}[f(t)]=\frac{d^{\beta}f(t)}{dt^{\beta}}=\frac{1}{\Gamma(1-\beta)}\frac{d}{dt}\left[\int_0^t\frac{f(\tau)}{(t-\tau)^{\beta}}d\tau\right] \tag{3}$$

The properties of the VED in frequency domain are more commonly used in analysis. It can be obtained by adopting Fourier transformation

$$\mathrm{F}\left(D^{\alpha}[f(t)]\right)=(i\bar{\omega})^{\alpha}\,\hat{f}(\bar{\omega}) \tag{4}$$

$$\mathrm{F}\left(D^{\beta}[f(t)]\right)=(i\bar{\omega})^{\beta}\,\hat{f}(\bar{\omega}) \tag{5}$$

where $\mathrm{F}(\ )$ is the Fourier transform operator, $\hat{f}(\bar{\omega})$ is the Fourier transform of time function $f(t)$.

Then the linear dynamic properties of materials in the frequency domain are characterized by the complex modulus and the relationship between force amplitude $\hat{P}(\bar{\omega})$ and displacement amplitude $\hat{u}(\bar{\omega})$ is obtained, which is:

$$\hat{P}(\bar{\omega})=[G_1(\bar{\omega})+iG_2(\bar{\omega})]\hat{u}(\bar{\omega}) \tag{6}$$

where $G_1(\bar{\omega})$ and $G_2(\bar{\omega})$ are the frequency dependent storage and loss stiffness of the damper respectively, given as follows

$$G_1(\bar{\omega})=\frac{k_0[1+b_0\bar{\omega}^{\beta}\cos(\frac{\beta\pi}{2})]+c_0\bar{\omega}^{\alpha}[\cos(\frac{\alpha\pi}{2})+b_0\bar{\omega}^{\beta}\cos(\frac{\alpha-\beta}{2}\pi)]}{1+{b_0}^2\bar{\omega}^{2\beta}+2b_0\bar{\omega}^{\beta}\cos(\frac{\beta\pi}{2})} \tag{7}$$

$$G_2(\bar{\omega})=\frac{-b_0k_0\bar{\omega}^{\beta}\sin(\frac{\beta\pi}{2})+c_0\bar{\omega}^{\alpha}[\sin(\frac{\alpha\pi}{2})+b_0\bar{\omega}^{\beta}\sin(\frac{\alpha-\beta}{2}\pi)]}{1+{b_0}^2\bar{\omega}^{2\beta}+2b_0\bar{\omega}^{\beta}\cos(\frac{\beta\pi}{2})} \tag{8}$$

The loss factor can be calculated by the following equation

$$\eta(\bar{\omega})=\frac{G_2(\bar{\omega})}{G_1(\bar{\omega})} \tag{9}$$

The damping coefficient to a specific excitation frequency is defined as

$$\mathrm{C}(\bar{\omega})=\frac{G_2(\bar{\omega})}{\bar{\omega}} \tag{10}$$

The undetermined parameters in Eqs. (7)and (8) can be obtained by fitting the experimental results. A total number of 26 tests were conducted by Makris and Constantinous (1991) in the range of 0.01-50Hz at a fixed room temperature (25 degrees Celsius). Parameter α was set equal to unity. Parameters b_0 and β were determined in a least-square fit of the elastic stiffness curve, which is defined as the square root of the sum of squares of $G_1(\bar{\omega})$ and $G_2(\bar{\omega})$. Constant c_0 was then found by fitting the damping coefficient curve, which is described as Eq. (10). Finally, the obtained parameters are k_0=0N/m, c_0=15kN/m, b_0=0.3s$^{0.6}$, α=1 and β=0.6, good agreement is achieved between the model and the test results.

The frequency dependent storage, loss stiffness and damping coefficient are shown in Fig. 1. The force displacement loop for different excitation frequencies are shown in Fig. 2.

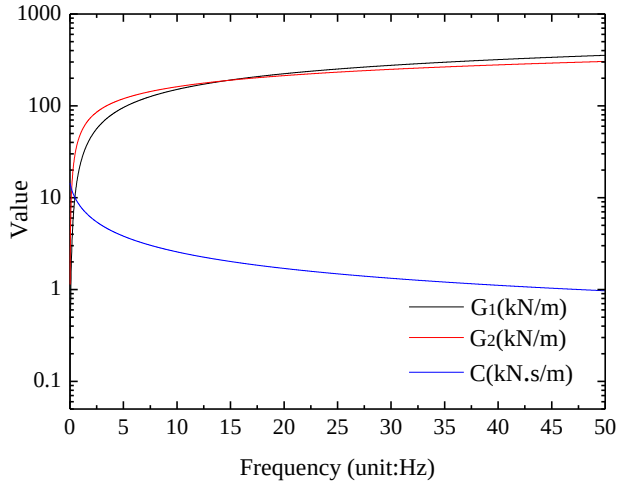

Fig. 1 Stiffness and damping coefficient of FDM

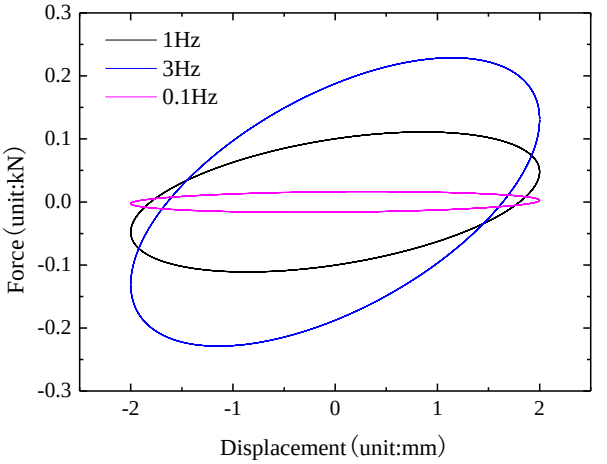

Fig. 2 The Force-Displacement loop of FDM

3. The mathematical model of the system

A wind resistant frame structural system equipped with TMD at the top floor and VEDs at the diagonal of each floor is considered. The superstructure is treated as an elastic linear system and could be simplified as the shear frame model. The mass of the system is lumped at the level of each story. The beams and columns are assumed to be axially inextensible so that the rotational nodal parameters from the equations of motion can be eliminated. Thus, the physical model of an *N*-storey frame structure with TMD installed at the top of the structure and VEDs equipped at each story considering the SSI effect can be simplified as shown in Fig. 3.

On the basis of the relevant literatures (Bielak 1976, Wolf 1989), the pile foundation impedance can be written in the frequency domain as follows

$$G_l(ia_0) = K_l\ (a_0) + iC_l\ (a_0) \tag{11}$$

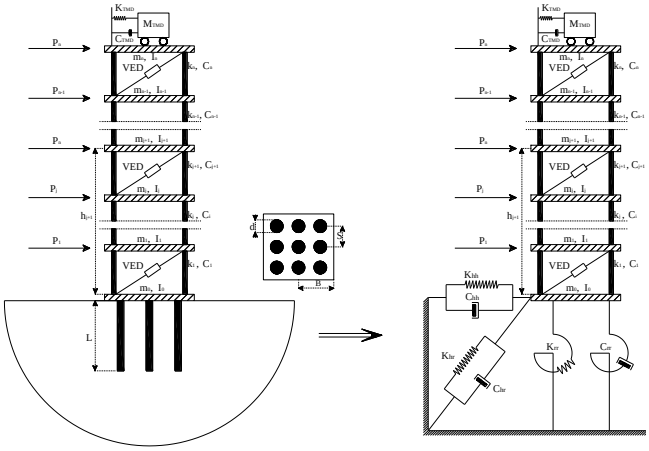

Fig. 3 The physical mode of frame structure equipped with TMD and VEDs considering SSI effect

In which $a_0 = \bar{\omega}B / V_s$ is the dimensionless frequency, where V_s represents the soil shear wave propagation velocity. The subscripts l is *hh*, *hr*, *rr* respectively. Thus, K_{hh}, K_{rr}, K_{hr} represent the swaying, rocking and the coupled swaying-rocking stiffness of the springs as illustrated in Fig. 3. C_{hh}, C_{rr} and C_{hr} represent the dashpots of the swaying, rocking and the coupled swaying-rocking of the corresponding springs. The frequency dependent numerical parameters of pile group dynamic impedance used in this paper are calculated by the method proposed by Gazetas *et al.* (1993).

The superstructure is founded on a square pile group embedded in a homogeneous, viscoelastic and isotropic half-space. It is assumed that the pile heads are clamped by the rigid pile cap which is considered as a rigid square plate of negligible thickness. The pile group parameters are denoted as follows: the pile length L and pile sectional diameter d , centre-to-centre spacing between adjacent piles S, cap mass m_0 and cap moment of inertia I_0, and the foundation half width B. The moment of inertia of the floor and cap can be calculated by the expressions $I=mb^2/3$ and $I_0=m_0B^2/3$ respectively (pile cap and structure mass is uniformly distributed over square area).

Firstly, the equilibrium equations of the system can be written in the time domain as follows

$$\boldsymbol{M\ddot{u}}+\boldsymbol{C\dot{u}}+\boldsymbol{Ku}+\boldsymbol{F}_{\mathrm{VED}} = f_{\mathrm{TMD}} + \boldsymbol{p}(t) \tag{12}$$

$$M_{\mathrm{TMD}}\ddot{u}_{\mathrm{TMD}} + C_{\mathrm{TMD}}(\dot{u}_{\mathrm{TMD}} - \dot{u}_N) + K_{\mathrm{TMD}}(u_{\mathrm{TMD}} - u_N) = 0 \tag{13}$$

$$f_{\mathrm{TMD}} = C_{\mathrm{TMD}}(\dot{u}_{\mathrm{TMD}} - \dot{u}_N) + K_{\mathrm{TMD}}(u_{\mathrm{TMD}} - u_N) \tag{14}$$

where

$$\boldsymbol{u}(t) = \{u_1(t), u_2(t), \cdots, u_k(t) \cdots, u_N(t), u_{TMD}(t), u_h(t), u_r(t)\} \tag{15}$$

$$\boldsymbol{p}(t)=\left\{p_1(t),p_2(t),\cdots,p_k(t)\cdots,p_N(t),0,\sum_i^N p_i(t),\sum_i^N p_i(t)\boldsymbol{H}(i)\right\} \quad (16)$$

In the above equations, the symbols $\boldsymbol{M}$, $\boldsymbol{C}$, $\boldsymbol{K}$ denote the mass, damping, and stiffness matrices of the system, respectively. M_{TMD}, C_{TMD} and K_{TMD} are the mass, damping and stiffness of the TMD and u_{TMD} represents the horizontal displacement of the TMD. The $\boldsymbol{p}(t)$ and $\boldsymbol{u}(t)$ are both $(N+3)$-dimensional vectors that represent the time history of the wind load and the displacement of the system, respectively. $\boldsymbol{H}$ represents the height vector of the structure and $u_{\mathrm{h}}(t)$ and $u_{\mathrm{r}}(t)$ represent the horizontal and rocking displacement of the cap.

If the structure is equipped with only one VED denoted as the damper number i, which is mounted between two successive stories j and $j+1$, then the force interaction vector $\boldsymbol{F}(t)$ could be written in the following form

$$\boldsymbol{F}(t)=\boldsymbol{F}_i(t)=[0,\cdots,F_j=f_i,F_{j+1}=-f_i,\cdots,0,0,0]^T=\boldsymbol{L}_i^T f_i(t) \quad (17)$$

where $\boldsymbol{L}_i=[0,\cdots,L_i=1,L_{i+1}=-1,\cdots,0,0,0]$ is the ith damper allocation vector of dimension $N+3$, $f_i(t)$ is the damper force in time domain.

For a structure with m dampers, the force interaction vector is given as follows

$$\boldsymbol{F}(t)=\sum_{i=1}^m \boldsymbol{F}_i(t)=\sum_{i=1}^m \boldsymbol{L}_i^{\mathrm{T}} f_i(t) \quad (18)$$

Eq. (17) can be written in frequency domain by Fourier transformation

$$\boldsymbol{F}(\bar{\omega})=\sum_{i=1}^m \boldsymbol{F}_i(\bar{\omega})=\sum_{i=1}^m \boldsymbol{L}_i^{\mathrm{T}} f(\bar{\omega})=\sum_{i=1}^m \boldsymbol{L}_i^{\mathrm{T}}[G_1(\bar{\omega})+iG_2(\bar{\omega})]\cos^2\theta_0\boldsymbol{L}_i\boldsymbol{U}(\bar{\omega}) \quad (19)$$

where $\boldsymbol{U}(\bar{\omega})$ represents the Fourier transform of $\mathbf{u}(t)$. θ_0 represents the installation angle of VED.

The equilibrium equations can be expressed in the frequency domain due to the frequency dependency of constitutive parameters of VED and the impedance function of pile group

$$\left\{-\bar{\omega}^2[\boldsymbol{M}]+j\bar{\omega}[\boldsymbol{C}]+[\boldsymbol{K}]\right\}\boldsymbol{U}(\bar{\omega})=\boldsymbol{P}(\bar{\omega}) \quad (20)$$

where

$$\boldsymbol{M}=\begin{pmatrix} \boldsymbol{M}_s & \mathbf{0}_{n\times1} & \boldsymbol{M}_s\boldsymbol{E} & \boldsymbol{M}_s\boldsymbol{H} \\ \mathbf{0}_{1\times n} & M_{TMD} & M_{TMD} & M_{TMD}H_{top} \\ \boldsymbol{E}^T\boldsymbol{M}_s & M_{TMD} & M_T & E_T \\ \boldsymbol{H}^T\boldsymbol{M}_s & M_T & E_T & I_T \end{pmatrix} \quad (21)$$

$$\boldsymbol{K}=\begin{pmatrix} \boldsymbol{K}_s+\boldsymbol{K}_d & K_{TMD}\boldsymbol{E} & \mathbf{0}_{n\times1} & \mathbf{0}_{n\times1} \\ \boldsymbol{E}^T K_{TMD} & K_{TMD} & 0 & 0 \\ \mathbf{0}_{1\times n} & 0 & K_{hh} & K_{hr} \\ \mathbf{0}_{1\times n} & 0 & K_{rh} & K_{rr} \end{pmatrix} \quad (22)$$

$$\boldsymbol{C}=\begin{pmatrix} \boldsymbol{C}_s+\boldsymbol{C}_d & C_{TMD}\boldsymbol{E} & \mathbf{0}_{n\times1} & \mathbf{0}_{n\times1} \\ \boldsymbol{E}^T C_{TMD} & C_{TMD} & 0 & 0 \\ \mathbf{0}_{1\times n} & 0 & C_{hh} & C_{hr} \\ \mathbf{0}_{1\times n} & 0 & C_{rh} & C_{rr} \end{pmatrix} \quad (23)$$

The symbols in the above matrices are expressed as follows

$$M_T=m_0+M_{TMD}+\sum_{i=1}^N \boldsymbol{M}_s(i,i) \quad (24)$$

$$E_T=M_{TMD}H_{top}+\sum_{i=1}^N \boldsymbol{M}_s(i,i)\cdot\boldsymbol{H}(i) \quad (25)$$

$$I_T=\boldsymbol{M}_{TMD}H_{top}^2+I_0+\sum_{i=1}^n[\boldsymbol{M}_s(i,i)\cdot\boldsymbol{H}^2(i)+I_{\mathrm{i}}] \quad (26)$$

$$\boldsymbol{K}_d(\bar{\omega})=\sum_{i=1}^m \boldsymbol{L}_i^{\mathrm{T}} G_1(\bar{\omega})\cos^2\theta_0\boldsymbol{L}_i \quad (27)$$

$$\boldsymbol{C}_d(\bar{\omega})=\sum_{i=1}^m \boldsymbol{L}_i^{\mathrm{T}}\frac{G_2(\bar{\omega})}{\bar{\omega}}\cos^2\theta_0\boldsymbol{L}_i \quad (28)$$

where $\boldsymbol{M}_{\mathrm{s}}$, $\boldsymbol{K}_{\mathrm{s}}$ and $\boldsymbol{C}_{\mathrm{s}}$ represent the matrix of the mass, stiffness and damping of the superstructure, $\boldsymbol{E}$ is a column vector of order N with each element being equal to unity. H_{top} represents the height of top floor from the cap, $\boldsymbol{U}(\bar{\omega})$ and $\boldsymbol{P}(\bar{\omega})$ are the corresponding Fourier transformation of $\boldsymbol{u}(t)$ and $\boldsymbol{p}(t)$.

Rayleigh proportional damping is considered in the research. Thus, the damping matrix of the structure $\boldsymbol{C}_{\mathrm{s}}$ can be expressed as linear combination of mass and stiffness matrices of the building

$$\boldsymbol{C}_{\mathrm{s}}=\alpha\boldsymbol{M}_{\mathrm{s}}+\beta\boldsymbol{K}_{\mathrm{s}} \quad (29)$$

where α and β are the Rayleigh damping coefficient.

The equilibrium equations can be solved in frequency domain programmatically and the time-history response of the structure are then obtained by inverse Fourier transform.

4. Simulation of the along-direction fluctuating wind load

Under the premise of satisfying practical precision in engineering, wind speed time history could be assumed as follows: (1) the average wind speed of any point does not change with time; (2) fluctuating wind speed time history is a stationary random process with mean value of 0; (3) wind speed time history is spatial correlated.

The Davenport spectrum is adopted as the wind speed power spectrum in this paper. This spectrum is based on more than 90 strong wind records measured at different

locations and different heights. The empirical formula could be expressed by Eq. (30)

$$S_v(f)=\frac{4kx^2\bar{v}_{10}^2}{f^2(1+x^2)^{3/4}} \tag{30}$$

where, k represents the ground surface roughness coefficient, f represents the frequency of the fluctuating wind and $\bar{v}_{10}$ represents the wind speed at 10 m from the ground. x denotes the turbulence integral scale coefficient, given as follows

$$x=1200\frac{f}{\bar{v}_{10}} \tag{31}$$

The Auto-regressive (AR) model method is used to simulate the multidimensional wind speed (Paola1998), the column vector of fluctuating wind speed time history $\boldsymbol{v}(\boldsymbol{X}, \boldsymbol{Y}, \boldsymbol{Z}, t)$ for M spatial correlated points is given as Eq. (32)

$$\boldsymbol{v}(\boldsymbol{X},\boldsymbol{Y},\boldsymbol{Z},t)=\sum_{k=1}^{p}\boldsymbol{\psi}_k\boldsymbol{v}(\boldsymbol{X},\boldsymbol{Y},\boldsymbol{Z},t-k\Delta t)+\boldsymbol{N}(t) \tag{32}$$

where, $\boldsymbol{X}=[x_1,\cdots,x_M]^T$, $\boldsymbol{Y}=[y_1,\cdots,y_M]^T$, $\boldsymbol{Z}=[z_1,\cdots,z_M]^T$, ($x_i$, y_i, z_i) is the coordinate of the ith spatial point; p is the order of AR model; Δt is the time step of simulating wind speed time history; $\boldsymbol{\psi}_k$ is the autoregressive coefficient matrix of AR model, which is an $M\times M$ square matrix; k=1,…, p; $\boldsymbol{N}(t)$ is the vector of independent random process, it can be obtained by Eq. (33)

$$\boldsymbol{N}(t)=\boldsymbol{L}\cdot\boldsymbol{n}(t) \tag{33}$$

where $\boldsymbol{n}(t)=[n_1(t),n_2(t),\cdots n_M(t)]^T$, n_i(t) is a normal distribution with mean value of 0 and variance of 1, i=1,…, M ; $\boldsymbol{L}$ is a lower triangular matrix of order M, which can be obtained by the Cholesky decomposion of $\boldsymbol{R}_N$ expressed as Eq. (36).

The relationship between the covariance $\boldsymbol{R}$ and regress coefficient $\boldsymbol{\psi}$ of random wind process can be expressed as follows

$$\boldsymbol{R}\cdot\boldsymbol{\psi}=\begin{bmatrix}\boldsymbol{R}_N\\ \boldsymbol{O}_p\end{bmatrix} \tag{34}$$

where

$$\boldsymbol{\psi}=[\boldsymbol{I},\psi_{1,}\cdots\psi_p]^T \tag{35}$$

$$\boldsymbol{R}_N=\boldsymbol{R}_0+\sum_{k=1}^{p}\boldsymbol{\psi}_k\boldsymbol{R}(k\Delta t) \tag{36}$$

where $\boldsymbol{\psi}$ is a $(p+1)M\times M$ matrix, $\boldsymbol{I}$ is an $M\times M$ identity matrix; $\boldsymbol{O}_p$ is an $M\times(p+1)M$ matrix, with all elements valued at 0. $\boldsymbol{R}$ is a $(p+1)M\times(p+1)M$ autocorrelation Toeplitz matrix, given as follows

$$\boldsymbol{R}=\begin{bmatrix} R_{11}(0) & R_{12}(\Delta t) & R_{13}(2\Delta t) & \cdots & R_{1(p+1)}(p\Delta t)\\ R_{21}(\Delta t) & R_{22}(0) & R_{23}(\Delta t) & \cdots & R_{2(p+1)}[(p-1)\Delta t]\\ R_{31}(2\Delta t) & R_{32}(\Delta t) & R_{33}(0) & \cdots & R_{3(p+1)}[(p-2)\Delta t]\\ \vdots & \vdots & \vdots & \vdots & \vdots\\ R_{(p+1)1}(p\Delta t) & R_{(p+1)2}[(p-1)\Delta t] & R_{(p+1)3}[(p-2)\Delta t] & \vdots & R_{(p+1)(p+1)}(0)\end{bmatrix}_{(p+1)M\times(p+1)M} \tag{37}$$

where, $\boldsymbol{R}_{ij}$ is an M×M identity matrix, it can be obtained by Wiener-Khintchine function

$$R_{ij}(\tau)=\int_0^{\infty}S_{ij}(f)\cos(2\pi f\tau)d\omega \tag{38}$$

If i=j, S_{ij}(f) represents the auto-power spectral density function of the fluctuating wind.

If i≠j S_{ij}(f) represents the cross-power spectral density function of the fluctuating wind which can be obtained by the following expressions

$$S_{ij}(f)=\sqrt{S_{ii}(f)S_{jj}(f)}\cdot r_{ij}(f) \tag{39}$$

where, $S_{ii}(f)$ or $S_{jj}(f)$ can use the Davenport spectrum proposed above, $r_{ij}(f)$ represents the spatial-temporal correlation of the wind time history.

Regress coefficient matrix $\boldsymbol{\psi}$ can be obtained by solving liner equations given by Eq.(34). In order to gain a stable result, Gauss Jordan elimination method is used. $\boldsymbol{R}_N$ can be obtained by Cholesky factorization. Then $\boldsymbol{N}(t)$ can be obtained, and Eq. (32) could be rewritten as

$$\begin{bmatrix}v^1(j\Delta t)\\ \vdots\\ v^M(j\Delta t)\end{bmatrix}=-\sum_{k=1}^{p}\boldsymbol{\psi}_k\cdot\begin{bmatrix}v^1[(j-k)\Delta t]\\ \vdots\\ v^M[(j-k)\Delta t]\end{bmatrix}+\begin{bmatrix}N^1(j\Delta t)\\ \vdots\\ N^M(j\Delta t)\end{bmatrix} \tag{40}$$

By solving the above equitation, we can obtain M temporal and spatial related wind speed time history with time interval Δt .

Then, the final wind speed at the height z is the combination of average wind speed $\bar{v}(z,t)$ and the fluctuating wind speed

$$V(z,t)=\bar{v}+\bar{v}(z,t) \tag{41}$$

According to Davenport, the average wind speed can be obtained by the following equation

$$\frac{\bar{v}}{\bar{v}_b}=\left(\frac{z}{z_b}\right)^{\alpha} \tag{42}$$

where $\bar{v}_b$ represents the wind speed at a standard height z_b .

5. The integrated optimization process

5.1 The numerical example

In this section, the optimization process is demonstrated by a 20-storey frame structure with uniform mass and stiffness distribution. The superstructure is supported by a square pile group foundation embedded in a homogeneous, viscoelastic

and isotropic half space. The width, depth and height of the structure are 30 m, 30 m, and 90 m respectively. The pile group foundation is assumed to be embed in three different types of soil: soft soil with 100 m/s shear wave velocity, medium soil with 250 m/s shear wave velocity, dense soil with 500 m/s shear wave velocity. The parameters of the superstructure are shown in Table 1. The parameters of the pile group foundation and soil are shown in Table 2.

The TMD is mounted on top floor and the VEDs are installed on the diagonal of each story with an installation angle $\pi/4$. The general parameters of the viscoelastic element obtained from experiment data have already been displayed in the previous section. The Rayleigh damping ratio is used for the superstructure with the first two modal damping ratios being equal to 0.02.

The Davenport along wind speed spectrum is used to generate the wind history and the duration of wind load is set to 800s. The fluctuating wind speed history on each floor of the building can be calculated through the method proposed in Section 4. Fig. 4 gives the time history of along wind speed on top floor.

Table 1 Parameters of the superstructure

Floor	***M*** (kg)	***K*** (kN/m)	***I*** $(kN{\cdot}m^2)$	***H*** (m)
1~4	3.2×10^5	3.5×10^8	4.52×10^7	4.5
5~10	3.2×10^5	3.0×10^8	4.52×10^7	4.5
11~16	3.2×10^5	2.5×10^8	4.52×10^7	4.5
17~20	3.2×10^5	2.2×10^8	4.52×10^7	4.5

Table 2 Parameters of pile and soil

Model	**Parameter**	**Symbol**	**Value**	**Unit**
Pile	pile configuration	$n\times n$	5×5	-
	cap mass	m_b	1.5×10^5	kg
	cap half side width	B	15	m
	cap moment of inertia	I_b	1.13×10^7	$kg\times m^2$
	pile diameter	d	1	m
	pile length	L	30	m
	pile space	S	7.5	m
	pile Young's modulus	E_p	2.4×10^4	Mpa
	pile density	ρ_b	2.5×10^3	kg/m^3
	pile Poisson's ratio	ν_b	0.25	-
Soil	Mass density	ρ_s	2×10^3	kg/m^3
	Poisson's ratio	ν_s	0.4	-
	shear velocity	V_s	100 /250 /500	m/s

Fig. 5 gives the comparison of the target spectrum and the simulation result. It can be seen from the figures that the simulation result can well match the target spectrum. The wind load on each floor can be obtained easily within consideration of the windward surface of the building.

5.2 The optimization procedure

Wind-induced serviceability is an important problem to be concerned in the structural design. It's considered to ensure the comfort of people. The comfort of the people is mainly dependent upon the acceleration of the building under wind load. Many countries have corresponding codes limiting the maximum wind-induced acceleration of the structure to meet the need of serviceability.

Consequently, the acceleration at the top of the building is chosen as the control objective in this research. The optimization problem can be defined as a procedure of finding the minimum acceleration at the top of the building in different parameter combinations of VEDs and TMD. Theoretically, the optimal solution for such a problem can be obtained by enumerable search of every possible combination of parameters since the design space is discrete.

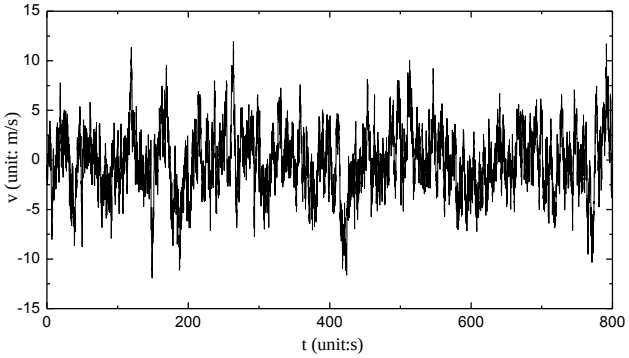

Fig. 4 Time history of wind velocity on the 20th floor of the building

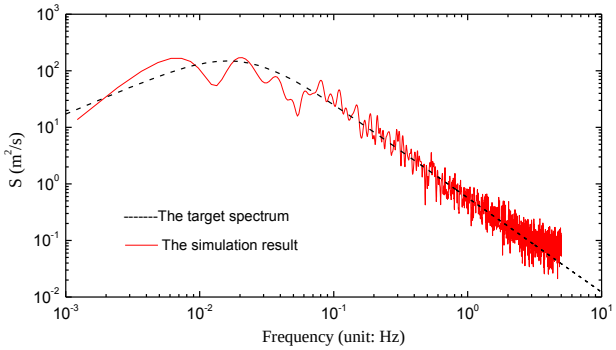

Fig. 5 The comparison of target spectrum and the simulation result

However, the practical implementation of this method is not at all effective due to large number of feasible design combinations. In order to solve the problem more effectively, the GA is adopted as a numerical searching technique to find the optimal results. The GA is an optimization technique simulating the evolutionary process based on the principles of natural biological evolutionary process where the stronger individuals are likely to be winners in a competing environment (Furuya *et al.* 1998). For the past few years, the GA has been successfully applied to a wide range of engineering applications and proved to be very effective in solving the discrete space optimization problems for its features of evolutionary, multi-point, direct and parallel searching.

In this study, binary code with 0 and 1 is employed to represent the parameters of TMD (KTMD, MTMD, ξ_{TMD}) and the parameter of VED (c0). The design variables can be encoded by mapping in a certain range using an n-bit of binary unsigned integer. The GA starts with an initial population, which comprises Ng randomly created binary strings.

The main optimization procedure is illustrated as Fig. 6. The evolution starts from a population of randomly generated individuals (K_{TMD}, M_{TMD}, ξ_{TMD}, c_0). The population in each iteration is called a generation. In each generation, the fitness of every individual in the population is evaluated. The more fit individuals are stochastically selected from the current population, and each individual's genome is modified (recombined and possibly randomly mutated) to form a new generation. The new generation of candidate solutions is then used in the next iteration of the algorithm.

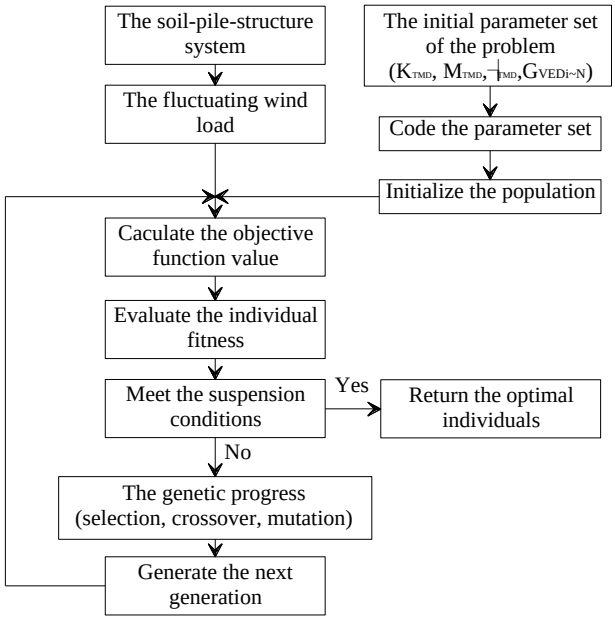

Fig. 6 The flow chart of the optimization process

The algorithm terminates when either a maximum number of generations has been produced or a satisfactory fitness level has been reached for the population.

In the application of GA, one population consists of 100 chromosomes (N_g=100), and each chromosome of the population is a string of size 16*n*. Selection is based on roulette wheel selection, the crossover operation is performed with a crossover probability of 0.8 and mutation operates with a mutation probability of 0.01.

The ranges of K_{TMD}, M_{TMD}, ξ_{TMD}, c_0 for the optimization process is set as follows based on the practical engineering

$$0.01\tilde{M}_1 \le M_{TMD} \le 0.1\tilde{M}_1 \tag{43}$$

$$0.1\tilde{\omega}_1 \le \omega_{TMD} \le 2\tilde{\omega}_1 \tag{44}$$

$$0.01 \le \xi_{TMD} \le 0.5 \tag{45}$$

$$0 \le c_0^i \le 0.5K_i \quad (i=1, 2, 3...N) \tag{46}$$

The response of superstructure without any control devices is firstly calculated as a comparison. Table 3 gives the peak response values and natural frequencies of the system without control devices for different soil types. For hard soil condition, the natural frequency of the system is almost the same as fixed base condition and the natural frequency decreases with soil softening. Fig. 7 gives the maximum acceleration and displacement of each floor for different soil types. It can be seen from figure that with the decrease of soil stiffness, the peak values of displacement and acceleration both increase.

Two cases of wind resistant system are considered as follows:

Case 1: Structure-TMD;

Case 2: Structure-TMD-VEDs.

The proposed design procedures illustrated by Fig.6 are applied to the system and the results are summarized as follows.

Fig. 8 shows the generation history of the optimization process of Case 2 for hard soil and soft soil conditions. The maximum acceleration of the top floor converges into its optimal value after approximately 250 generations.

Table 4 gives the optimal parameters of TMD for Case 1 under different soil conditions.

Table 3 The peak response value and natural frequencies of the system without control devices for different soil types

	Fixed base	**Hard soil**	**Medium soil**	**Soft soil**
Peak Displacement (*m*)	0.14	0.15	0.22	0.28
Peak Acceleration (m/s^2)	0.79	0.81	1.10	1.26
Frequency(*rad/s*)	1.98	1.96	1.89	1.75

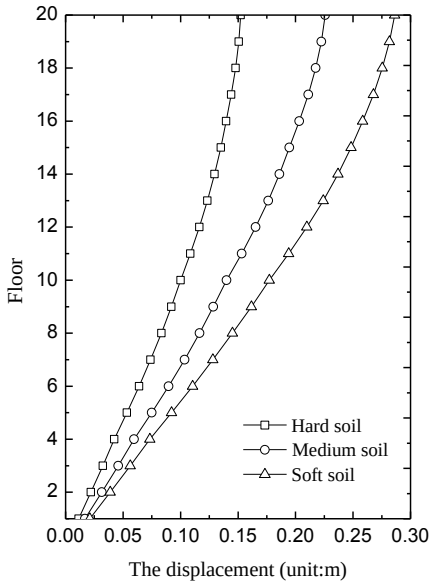

(a) The displacement

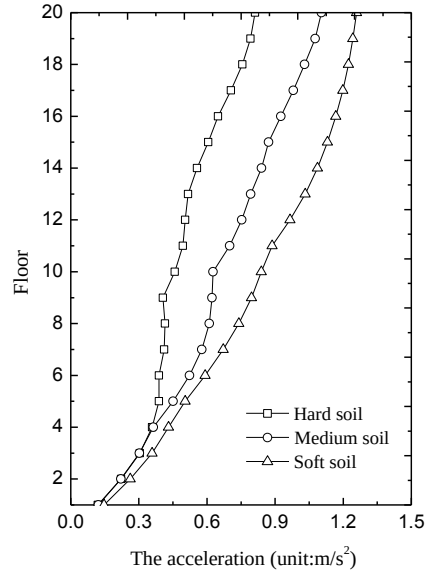

(b) The acceleration

Fig. 7 The maximum displacement and acceleration of each floor without control devices

The reduction amplitude in the table is defined as the ratio of reduction amount of acceleration or displacement to the original ones for structures without any control devices. Therefore, the devices have a better control effect if the reduction amplitude is higher.

The results given in Table 4 demonstrate that:

(1) The optimal parameters of TMD for hard soil condition are almost consistent with that for fixed base condition. It suggests that if structures are founded on hard soil, the SSI effect can be ignored and the optimal parameters of TMD obtained on assumption of rigid base are feasible ;

(2) The optimal frequency of the TMD ω_{TMD} is close to the natural frequency of the system, which is in agreement with the existing conclusions. Thus, the correctness of the optimization algorithm is verified;

(3) With soil softening, the optimal frequency of the TMD decreases due to the decrease of the natural frequency of the system caused by the SSI effect. It explains that the optimization procedure can sensitively capture the change of the dynamic characteristic of the system;

(4) Although the TMD can greatly reduce the structural acceleration and displacement for all soil conditions. According to the Chinese code, the allowable maximum acceleration of building under wind load is $0.25m/s^2$. It seems that the optimization results cannot meet the requirement for all soil conditions if the structure installed with TMD only.

Table 5 gives the optimal parameters of TMD for Case 2 under different soil conditions and Figs. 9-11 give the corresponding optimal distribution of VEDs at each floor.

Obviously, the integrated use of TMD and VEDs in structure have a better control of the top floor acceleration for all soil conditions compared with the structure installed with TMD only. The accelerations are also restricted to the allowable ranges for all soil conditions. The optimal frequency of the TMD has an increase compared with Case 1. The phenomenon describes that the VEDs provide additional stiffness of the system, which leads to an increase of the natural frequency of the system. Consequently, the optimization procedure captures the changes and gives the optimal results adaptable to the system. The optimal mass of TMD also has a large extend of decrease compared with Case 1.

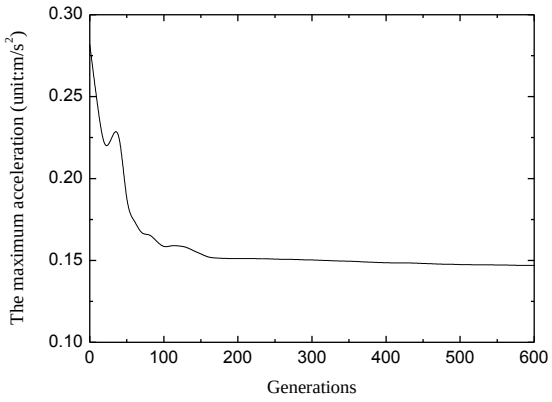

(a) Hard soil

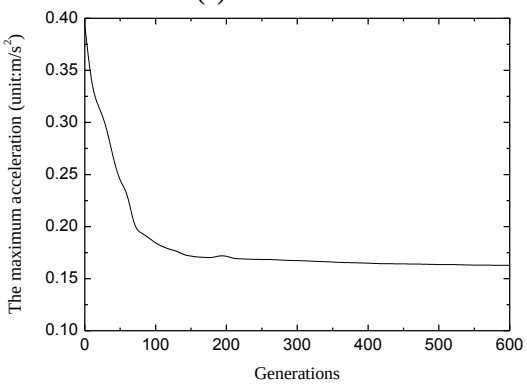

(b) Soft soil

Fig. 8 Generation history of the maximum acceleration of top floor

Table 4 The optimal parameters of TMD for Case 1

Soil types	Mass M_{TMD} (kg)	Damping ratio ξ_{TMD}	Stiffness K_{TMD} (kN/m)	Frequency ω_{TMD} (rad/s)	A_{max} (m/s^2)	Reduction amplitude
Fixed base	2.19×10^5	0.26	8.40×10^5	1.96	0.24	69.6%
Hard soil	2.18×10^5	0.25	8.33×10^5	1.95	0.25	69.1%
Medium soil	2.23×10^5	0.26	8.14×10^5	1.91	0.28	74.5%
Soft soil	2.68×10^5	0.28	7.89×10^5	1.71	0.34	73.1%

Table 5 The optimal parameters of TMD for Case 2

Soil types	Mass M_{TMD} (kg)	Damping ratio ξ_{TMD}	Stiffness K_{TMD} (kN/m)	Frequency ω_{TMD} (rad/s)	A_{max} (m/s^2)	Reduction amplitude
Fixed base	2.85×10^4	0.30	1.26×10^5	2.10	0.13	83.5%
Hard soil	2.87×10^4	0.29	1.24×10^5	2.08	0.13	84.0%
Medium soil	9.79×10^4	0.41	3.82×10^5	1.98	0.15	86.3%
Soft soil	9.04×10^4	0.30	3.45×10^5	1.95	0.16	87.3%

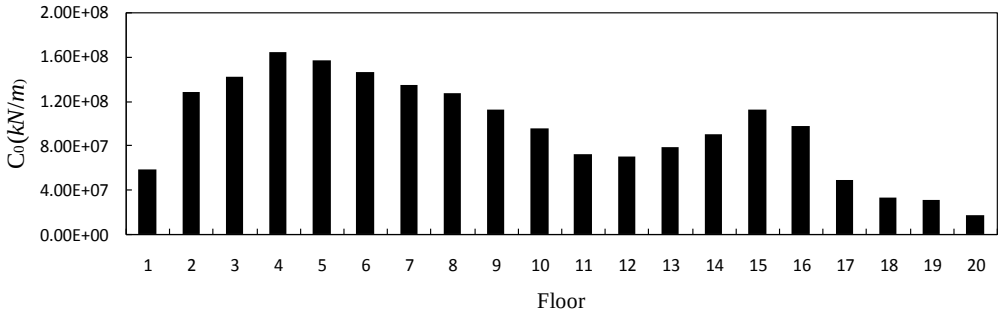

Fig. 9 The optimal distribution of the VEDs for Hard soil case (V_s=500 m/s)

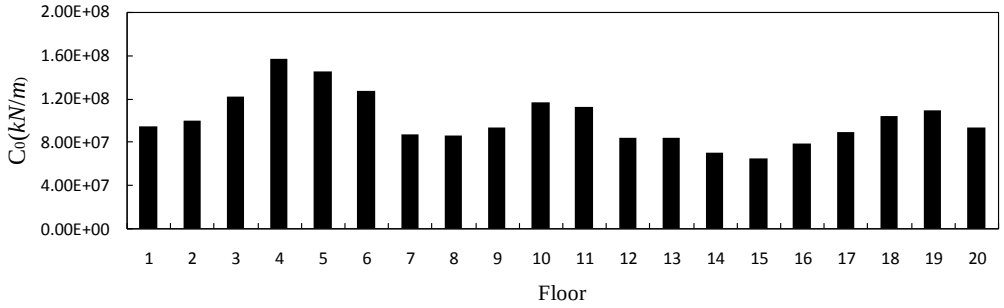

Fig. 10 The optimal distribution of the VEDs for Medium soil case (V_s=250 m/s)

Figs. 12 and13 give comparisons of acceleration and displacement among different control cases for three types of soil. It is evident from these figures that the integrated optimal design of TMD and VEDs has a best control of the system for all soil conditions. For structures with lower stiffness and damping, the combined use of TMD and VEDs seems a good choice for wind induced vibration control.

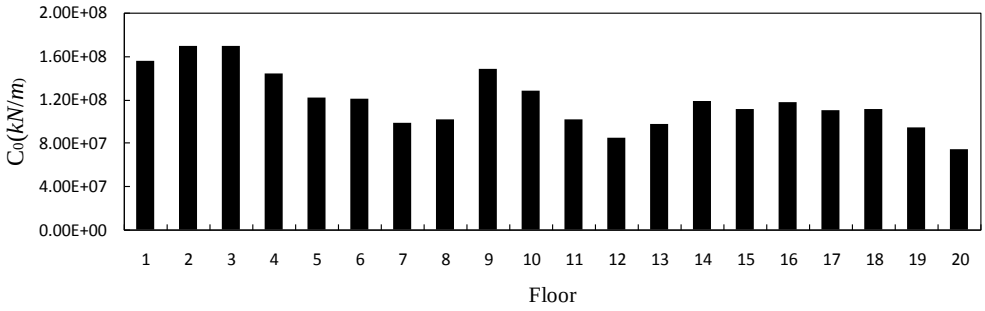

Fig. 11 The optimal distribution of the VEDs for Soft soil case (V_s=100 m/s)

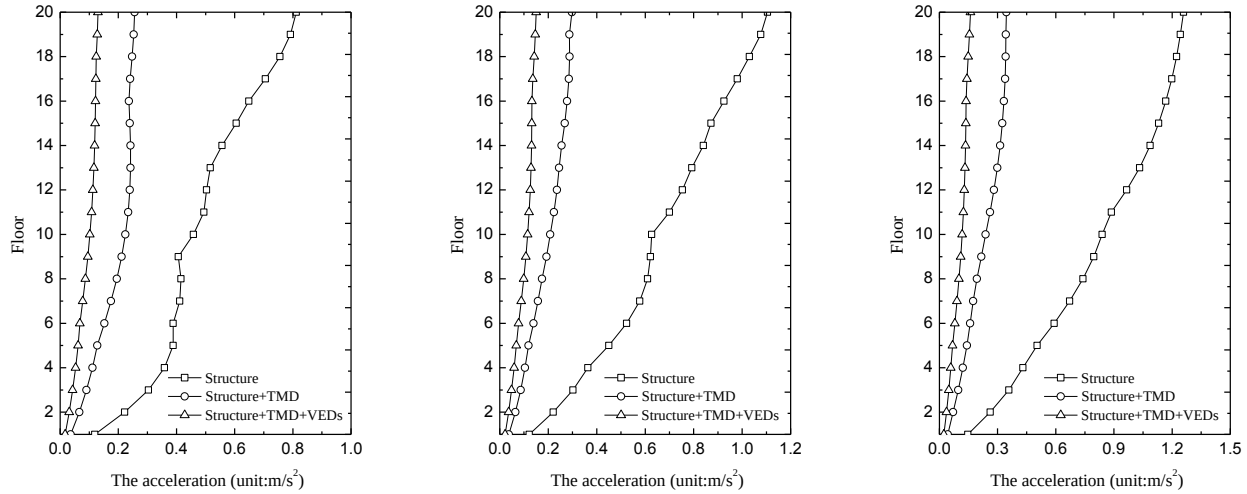

(a) Hard soil (b) Medium soil (c) Soft soil

Fig. 12 The comparison of acceleration for different cases

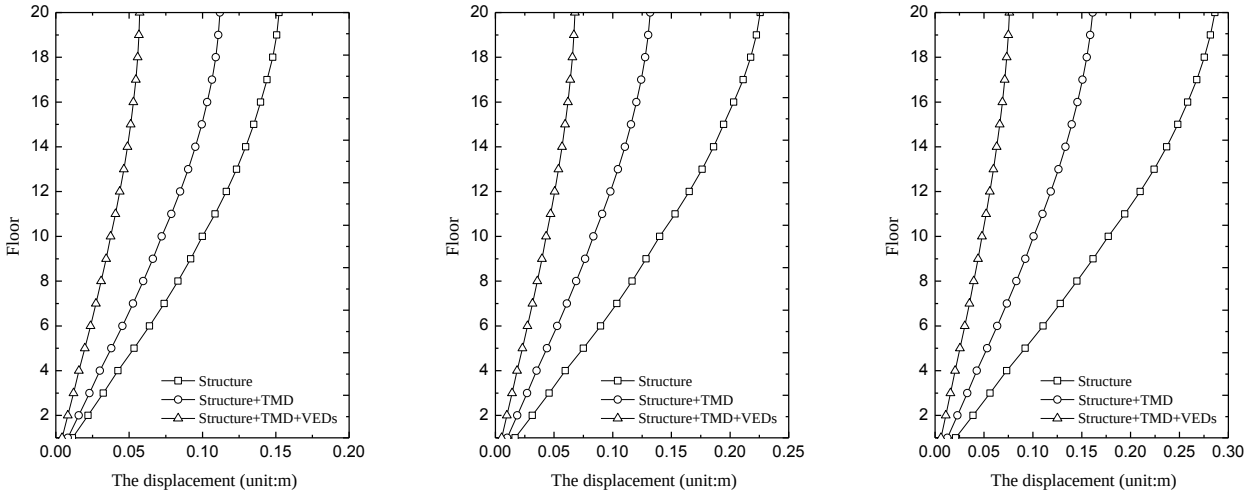

(a) Hard soil (b) Medium soil (c) Soft soil

Fig. 13 The comparison of displacement for different cases

6. Conclusions

The structural analysis considering SSI effect is usually realized by finite element software such as ABAQUS or ANSYS in the practical construction design and large amount of soil element needs to be established to get relatively accurate results. For optimization problems, it will takes a considerable amount of time.

The superstructure computational model can be idealized as a multiple-degree-of-freedom system with lumped masses in series linked by line elements for structures with relatively uniform mass and stiffness distribution. In the past few decades, there has been a more in-depth academic research on soil impedance function. Accordingly, the numerical parameters of soil impedance can be conveniently applied to equations of SSI system in frequency domain. Based on genetic algorithm, a rapid determination of the best parameters of TMD and VEDs for wind vibration control of frame structures considering the SSI effect can be obtained in frequency domain .

A 20-storey pile group supported frame structure is used as a numerical example to demonstrate the optimization process proposed in this paper. Through the numerical analysis, some conclusions can be draw from the investigation:

- The acceleration and displacement response of the structure excited by along-direction fluctuating wind without any control device have a tendency of increase with the soil softening.
- The optimal frequency of TMD is close to the natural frequency of the system. With the decrease of the soil stiffness, the best control frequency of TMD decreases as a result of the decline of the natural frequency of the system caused by the SSI effect.
- The optimization procedure can sensitively capture the changes of the dynamic characteristic of the system and give the best parameters for structural vibration control.
- The integrated optimal use of TMD and VEDs has a better control of the structural acceleration and displacement compared with the case that the structure installed with TMD only.

Acknowledgments

The authors are grateful for the financial support from National Natural Science Foundation of China (Grant no.90815017) .

References

Arfiadi, Y. and Hadi, M.N.S. (1998), "Optimum design of absorber for MDOF structures", *J. Struct. Eng.*, **124**(11), 1272-1280. https://doi.org/10.1061/(ASCE)0733-9445(1998)124:11(1272).

Avilés, J. and Pérez, L.E.(1996), "Evaluation of interaction effects on the system period and system damping due to foundation embedment and layer depth", *Soil Dynam. Earthq. Eng.*, **15**(1), 11-27. https://doi.org/10.1016/0267-7261(95)00035-6.

Ayorinde, E.O. and Warbuiron, G.B. (1980), "Optimum absorber parameters for simple systems", *Earthq. Eng. Struct. D.*, **8**(3), 197-217. https://doi.org/10.1002/eqe.4290080302.

Bekdaş, G. and Nigdeli, S.M. (2011), "Estimating optimum parameters of tuned mass dampers using harmony search", *Eng. Struct.*, **33**(9), 2716-2723. https://doi.org/10.1016/j.engstruct.2011.05.024.

Bekdaş, G. and Nigdeli, S.M. (2011)," "Investigation of SDOF idealization for structures with optimum tuned mass dampers", *Proceedings of the NaturalCataclysms and Global Problems of the Modern Civilization Geocataclysms*, September 19-21, Istanbul, Turkey.

Bielak, J.(1976), " Modal analysis for building-soil interaction" , *J. Eng. Mech. Division*, **102**(5), 771-786.

Brock, J.E. (1946), "A note on damped vibration absorber", *J. Appl. Mech*.

Chang, C.C. (1999), "Mass dampers and their optimal design for building vibration control", *Eng. Struct.*, **21**(5), 454-463. https://doi.org/10.1016/S0141-0296(97)00213-7.

Chang, K.C. and Lin, Y.Y. (2004), "Seismic response of full-scale structure with added viscoelastic dampers", *J. Struct. Eng.*, **130**(4), 600-608. https://doi.org/10.1061/(ASCE)0733-9445(2004)130:4(600).

Den Hartog, J.P. (1947), *Mechanical Vibrations*, McGraw-Hill, New York, NY, USA.

Desu, N.B., Deb, S.K. and Dutta, A. (2006), "Coupled tuned mass dampers forcontrol of coupled vibrations in asymmetric buildings", *Struct. Control Health Monit.*, **13**(5), 897-916. https://doi.org/10.1002/stc.64.

Furuya, O., Hamazaki, H. and Fujita, S. (1998), "Proper placement of energy absorbing devices for reduction of wind-induced vibration caused in high-rise buildings", *J. Wind Eng. Ind. Aerod.*, **98**(71), 931-942.

Gazetas, G., Fan, K. and Kaynia, A. (1993), "Dynamic response of pile groups with different configuration", *Soil Dynam. Earthq. Eng.*, **12**(4), 239-257. https://doi.org/10.1016/0267-7261(93)90061-U.

Hwang, J., Huang, Y., Yi S. and Ho, S. (2008), "Design formulations for supplemental viscous dampers to building structures" , *J. Struct.Eng.*, **134**(1), 22-31. https://doi.org/10.1061/(ASCE)0733-9445(2008)134:1(22).

Leung, A.Y.T., Zhang, H., Cheng, C.C. and Lee, Y.Y. (2008), "Particle swarmoptimization of TMD by non-stationary base excitation duringearthquake", *Earthq. Eng. Struct. D.*, **37**(9), 1223-1246. https://doi.org/10.1002/eqe.811.

Leung, A.Y.T. and Zhang, H. (2009), "Particle swarm optimization of tuned mass dampers", *Eng. Struct.*, **31**(3), 715-728. https://doi.org/10.1016/j.engstruct.2008.11.017.

Lewandowski, R., Bartkowiak, A. and Maciejewski, H.(2012), "Dynamic analysis of frames with viscoelastic dampers: a comparison of damper models", *Struct. Eng. Mech.*, **41**(1), 113-137. http://dx.doi.org/10.12989/sem.2012.41.1.113.

Makris, N. and Constantinou, M.C. (1991), " Fractional derivative Maxwell model For viscous dampers", *J. Struct. Eng.*, **117**(9), 2708-2724. https://doi.org/10.1061/(ASCE)0733-9445(1991)117:9(2708).

Marano, G.C., Greco, R. and Chiaia, B. (2010), "A comparison between differentoptimization criteria for tuned mass dampers design" , *J. Sound Vib.*, **329**(23), 4880-4890. https://doi.org/10.1016/j.jsv.2010.05.015.

Medina, C. and Aznárez J.J.(2013), "Effects of soil-structure interaction on the dynamic properties and seismic response of piled structures" , *Soil Dynam. Earthq. Eng.*, **53**(7), 160-175. https://doi.org/10.1016/j.soildyn.2013.07.004.

Nigdeli, S.M. and Bekdaş, G. (2011), "Optimization of tuned mass damper parameters for structures subjected to earthquakes with

forward directivity," In: *Natural Cataclysms and Global Problems of the Modern Civilization Geocataclysms*, September 19-21, Istanbul,Turkey.

Paola, M.D. (1998), "Digital simulation of wind field velocity", *J. Wind Eng. Ind. Aerod.*, **74-76**, 91-109. https://doi.org/10.1016/S0167-6105(98)00008-7.

Pourzeynali, S., Lavasani, H.H. and Modarayi, A.H. (2008), "Active control of highrise building structures using fuzzy logic and genetic algorithms", *Eng. Struct.*, **29**(3), 346-357. https://doi.org/10.1016/j.engstruct.2006.04.015.

Singh, M.P., Singh, S. and Moreschi, L.M. (2002), "Tuned mass dampers forresponse control of torsional buildings", *Earthq. Eng. Struct. D.*, **31**(4), 749-769. https://doi.org/10.1002/eqe.119.

Steinbuch, R. (2011), "Bionic optimisation of the earthquake resistance of high buildings by tuned mass dampers", *J. Bionic Eng.*, **8**(3), 335-344.

Veletsos, A.S. and Meek, J.W. (1974), "Dynamic behavior of building-foundation systems", *Earthq. Eng. Struct. D.*, **3**(2), 121-138. https://doi.org/10.1002/eqe.4290030203.

Wolf, J.P.(1989), "Soil-structure-interaction analysis in time domain", *Nuclear Eng. Design*, **111**(3), 381-393. https://doi.org/10.1016/0029-5493(89)90249-5.

Warburton, G.B. and Ayorinde, E.O. (1980), "Minimizing structural vibrations with absorbers", *Earthq. Eng. Struct. D.*, **8**(3), 219-236. https://doi.org/10.1002/eqe.4290080303.

Zhang, R.H. and Soong, T.T. (1992), "Seismic design of viscoelastic dampers for structural applications", *J. Struct. Eng.*, **118**(5), 1375-1392. https://doi.org/10.1061/(ASCE)0733-9445(1992)118:5(1375).

AD